Application of Fiber Optic Sensor and Piezoelectric Actuator to Flutter Suppression

Do-Hyung Kim,* Jae-Hung Han,† and In Lee‡
Korea Advanced Institute of Science and Technology, Daejeon 305-701, Republic of Korea

Introduction

FOR lightweight and flexible structures, it is important to measure and suppress the flow-induced vibrations caused by interactions between fluid and structures. Dynamic aeroelastic instabilities, such as flutter, involve the interaction of aerodynamic, inertia, and elastic forces of flight structures. Because flutter may cause disastrous structural failures in flight, the prediction of stability boundary and the suppression of flutter are very important analysis issues for flight structures.

In recent years, several active control strategies have been studied to modify favorably the behavior of aeroelastic systems using smart material and structure technologies. Lazarus et al.[1] successfully applied multi-input/multi-output controls to suppress vibration and flutter of a platelike lifting surface with surface-bonded piezoelectric actuators. Han et al.[2] performed numerical and experimental investigation on active flutter suppression of a swept-back cantilevered plate. Application of piezoelectric actuation to flutter control of a more realistic wing model was achieved under the Piezoelectric Aeroelastic Response Tailoring Investigation program at NASA Langley Research Center.[3]

Recently, fiber bragg grating (FBG) sensors have been increasingly studied for a variety of applications: health monitoring, vibration measurement, nondestructive testing and so on. Gratings are simple, intrinsic sensing elements that can be photoinscribed into a silica fiber and have the same advantages normally attributed to fiber sensors. In addition, the devices have an inherent self-referencing capability and are easily multiplexed in a serial fashion along a single fiber.[4] An overview of FBG sensors and systems is presented in Ref. 4. This paper investigates dynamic application of an FBG sensor system to the flutter suppression of a composite plate structure. In practical situations, the modeling of an aeroelastic system is complicated and the dynamic characteristics of an aeroelastic system changes with respect to the airflow speed. Therefore, the adaptiveness and the robustness are key features for an aeroelastic control system. A neuroadaptive feedback control algorithm is used in this study. The control system consists of the neuroidentification model and the neurocontroller. The real-time implementation of the adaptive controller is performed using a digital signal processing (DSP) board. The effectiveness of the flutter suppression system is evaluated via wind-tunnel testing.

System Description

The test model is a swept-back cantilevered composite plate with a surface-bonded FBG sensor and piezoceramic actuators. The base structure is graphite/epoxy (CU-125 NS, Hankuk Fiber) $[90_2/0_2]_s$ laminate. Two piezoceramics (C-82, Fuji Ceramics) and one FBG sensor (gauge length = 10 mm and $\lambda_B = 1546$ nm) are bonded on the root region as shown in Fig. 1. The principle of the FBG sensor is the measurement of the changes in reflective signal, which is the center wavelength of back-reflected light from a Bragg grating. The signal depends on the effective refractive index of the core and the periodicity of the grating. The wavelength detection mechanism used in the present study is based on two cavity lengths in Fabry–Perot readout interferometers to produce two quadrature phase-shifted signals from the Bragg grating sensor.[5] The detailed description may be found in Refs. 5 and 6.

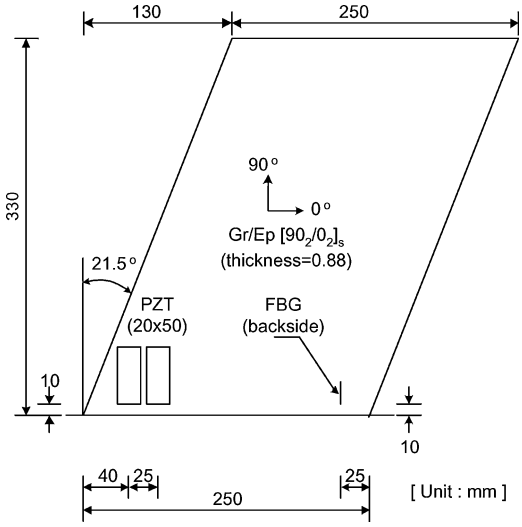

Fig. 1 Schematic diagram of the test model.

The neuroadaptive controller used in the present study is similar to the authors' previous work.[7] The network consists of one input vector and two layers: one hidden layer and one output layer. Tangent sigmoid and linear transfer functions were used for hidden and output layers, respectively. The error backpropagation learning rule is used, and the momentum method is applied to improve convergence characteristics and the convergent speed.

The control system consists of the neuroidentification model and the neurocontroller, and the overall architecture of the controller is shown in Fig. 2. The role of the neural network model (identifier) for the plant is to obtain mathematical representation of the real plant. The weights of the neural network model are adjusted so that the output of the neural network model should be the same as that of the plant. After completing the forward modeling, the tuning for weights of the neurocontroller is performed. Because the desired output value of the neurocontroller is not given in advance, this value should be calculated by the error backpropagation through the neural network plant model. The designed neural network controller is implemented using a DSP board (DS1102, dSPACE), and the weights are updated at every 0.01 s.

Results and Discussion

The wind-tunnel test has been performed in the subsonic wind tunnel at the Department of Aerospace Engineering, Korea Advanced Institute of Science and Technology. The wind tunnel is an open-circuit tunnel with effective speed ranges of 9–60 m/s and closed test section. First, aeroelastic responses to the airflow are investigated and the flutter prediction parameters are evaluated using sampled data. Then, flutter suppression experiments are performed at airflow velocities that cause limit-cycle oscillations for the uncontrolled case.

When the airflow speed is below 14.0 m/s, air damping is dominant, and the aeroelastic system is stable. As the airflow speed increases, the limit-cycle oscillation occurs, and the vibration amplitude increases. Power spectra of the FBG sensor data vs airflow speed are shown in Fig. 3. It can be seen that the vibration energy is concentrated in the second mode, which is the flutter mode, and increases according to the airflow speed.

Received 21 June 2003; revision received 18 November 2003; accepted for publication 18 November 2003. Copyright © 2003 by the American Institute of Aeronautics and Astronautics, Inc. All rights reserved.Copies of this paper may be made for personal or internal use, on condition that the copier pay the $10.00 per-copy fee to the Copyright Clearance Center, Inc., 222 Rosewood Drive, Danvers, MA 01923; include the code 0021-8669/04 $10.00 in correspondence with the CCC.

*Graduate Research Assistant, Department of Aerospace Engineering, 373-1 Guseong-dong, Yuseong-gu.

†Assistant Professor, Department of Aerospace Engineering, 373-1 Guseong-dong, Yuseong-gu.

‡Professor, Department of Aerospace Engineering, 373-1 Guseong-dong, Yuseong-gu; inlee@asdl.kaist.ac.kr. Senior Member AIAA.

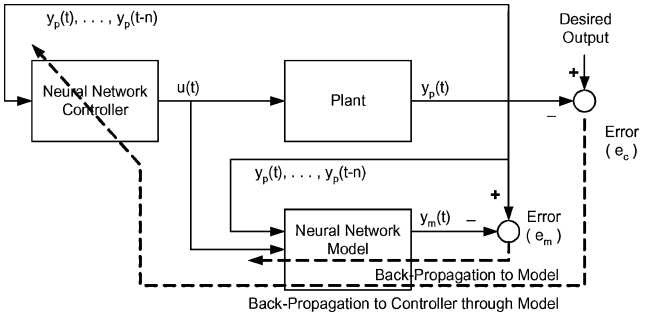

Fig. 2 Overall architecture for neurocontroller with neural network model.

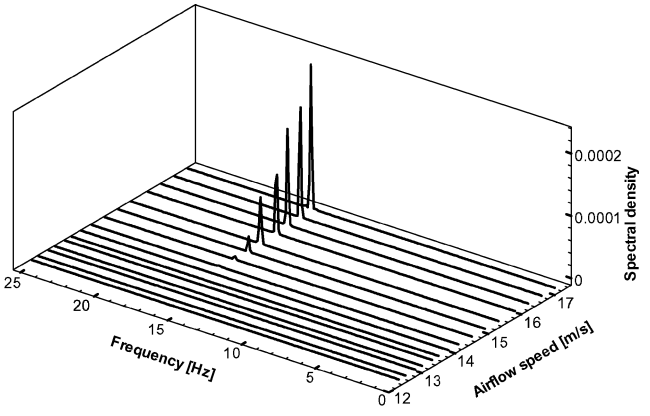

Fig. 3 Power spectra vs airflow speed.

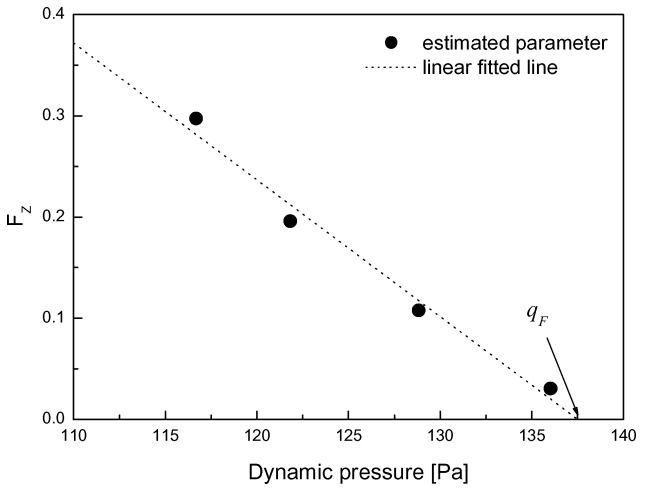

Fig. 4 Evaluated flutter prediction parameters.

In the process of aeroelastic analysis, the aeroelastic system is regarded as a linear system. Therefore, the flutter instability occurs and the stability boundary is clearly identified. However, in the experiment, there can be a limit-cycle oscillation region due to structural or aerodynamic nonlinear forces. Accordingly, the flutter speed for the actual system is not clearly defined, and it is difficult to determine the exact stability boundary. In addition, limit-cycle oscillations may lead to fatigue failure of an aeroelastic system. Therefore, the prediction of the dynamic aeroelastic stability boundary using experimental data that are sampled below the critical speed is very important and practical. The stability boundary has been evaluated using the flutter prediction parameter, F_z, proposed by Torri and Matsuzaki.[8] The flutter prediction parameters using experimental data vs dynamic pressure are shown in Fig. 4. The evaluated flutter speed is $V_F = 15.0$ m/s, which is close to the analytic result; the analytical flutter speed predicted using MSC/NASTRAN is $V_F = 15.4$ m/s.

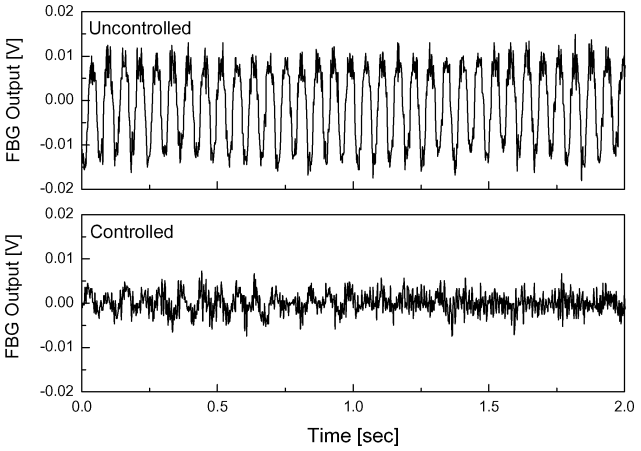

a) Time history

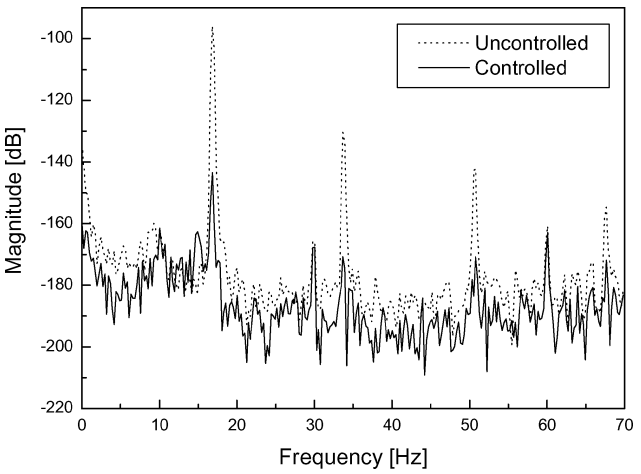

b) Power spectrum

Fig. 5 Flutter suppression result at $U_\infty = 17.0$ m/s.

The flutter suppression experiment has been performed at an airflow speed above the flutter boundary speed. Figure 5 shows the control results at $U_\infty = 17.0$ m/s. The effectiveness of the control system can be seen in both time and frequency domains. The amplitudes of the flutter mode and its harmonics are significantly reduced.

Conclusions

The present study investigates dynamic application of an FBG sensor system and the adaptive flutter control of a swept-back composite plate using a surface-bonded FBG sensor and piezoelectric actuators. The FBG sensor signal is used for the identification of the aeroelastic stability boundary as well as the suppression of flutter. The flutter prediction parameter calculated using sampled FBG sensor data accurately provides the stability boundary of an aeroelastic system. The real-time neuroadaptive control algorithm effectively reduces the amplitude of the flutter mode. The stability boundary and reliability of an aeroelastic system could be increased by integrating smart materials into advanced structures.

Acknowledgement

The present study has been supported by a grant from the National Research Laboratory Program of the Ministry of Science and Technology, Republic of Korea. The authors gratefully acknowledge this support (Subject 2000-N-NL-01-C-250).

References

[1]Lazarus, K. B., Crawley, E. F., and Lin, C. Y., "Multivariable Active Lifting Surface Control Using Strain Actuation: Analytical and Experimental Results," *Journal of Aircraft*, Vol. 34, No. 3, 1997, pp. 313–321.

[2]Han, J.-H., Tani, J., and Lee, I., "Flutter Suppression of a Lifting Surface Using Piezoelectric Actuation," *Proceedings of the Second Asian-Australasian Conference on Composite Materials*, The Korean Society for Composite Materials, Daejeon, Korea, 2000, pp. 843–848.

[3]Heeg, J., "Analytical and Experimental Investigation of Flutter Suppression by Piezoelectric Actuation," NASA TP-3241, Feb. 1993.

[4]Kersey, A. D., Davis, M. A., Patrick, H. J., LeBlanc, M., Koo, K. P., Askins, C. G., Putnam, M. A., and Friebele, E. J., "Fiber Grating Sensors," *Journal of Lightwave Technology*, Vol. 15, No. 8, 1997, pp. 1442–1463.

[5]Kim, C. G., Kim, D. H., and Hong, C. S., "Development of FBG Sensor System for Measuring the High Frequency Vibration of Structures and the Natural Frequency of Composites," *US–Korea Joint Workshop on Smart Infra-Structural Systems*, Smart Infra-Structure Technology Center, Daejeon, Korea, 2002, pp. 3–9.

[6]Lo, Y.-L., "In-Fiber Grating Sensors Using Interferometric Interrogating for Passive Quadrature Signal Processing," *IEEE Photonics Technology Letters*, Vol. 10, No. 7, 1998, pp. 1003–1005.

[7]Youn, S.-H., Han, J.-H., and Lee, I., "Neuro-Adaptive Vibration Control of Composite Beams Subject to Sudden Delamination," *Journal of Sound and Vibration*, Vol. 238, No. 2, 2000, pp. 215–231.

[8]Torri, H., and Matsuzaki, Y., "Flutter Margin Evaluation for Discrete-Time Systems," *Journal of Aircraft*, Vol. 38, No. 1, 2001, pp. 42–47.

Convergence of the Subsonic Doublet Point Method

L. H. van Zyl*
Defencetek, CSIR, Pretoria 0001, South Africa
and
T. Ueda†
Japan Aerospace Exploration Agency, Tokyo 182-8522, Japan

Nomenclature

C_l = lift coefficient
C_m = pitching moment coefficient
h = plunge amplitude
k = reduced frequency based on wing semispan
k_r = reduced frequency based on mean wing semichord
M = Mach number
n = number of boxes in aerodynamic model
n_y = number of spanwise strips on wing
s = wing semispan

Introduction

THE subsonic doublet point method[1] (DPM) is a simpler method compared to the subsonic doublet lattice method[2–4] (DLM) and offers computational efficiency at the cost of physical detail. In particular, it avoids the necessity of spanwise integration of the kernel functions but loses the representation of sweep by individual aerodynamic boxes. However, both methods should converge to the same result in the limit of infinitely small aerodynamic boxes. It was stated in Ref. 5 that the test cases used in Ref. 1 did not address the differences between the DPM and the DLM adequately, particularly with respect to sweep. The present work aims to give an indication of the effect of how this property is represented in the DPM compared to the DLM using some of the test cases suggested in Ref. 5. Note that the convergence of the subsonic DLM is almost linear with box size when the chordwise and spanwise paneling is refined simultaneously.[6] The same property is shown to exist for the doublet point method. Three test cases are considered: the AGARD wing and tail, a 70-deg delta wing, and a circular wing.

AGARD Wing and Tail

The unsteady lift coefficient of the AGARD wing and tail in plunge at $M = 0.8$ and $k_r = 1.2$ was calculated using the DLM and DPM and the same series of successively finer grids as was used in Ref. 6. The aerodynamic grids were generated using the minimum number of boxes while satisfying restraints on maximum box aspect ratio and maximum box chord. Box aspect ratios of 8, 2, and 0.5 were specified. A series of successively finer grids were generated for each aspect ratio by specifying a range of decreasing box chords. Figure 1 shows the convergence histories of the DLM and DPM results. The results are plotted against $1/\sqrt{n}$, which is proportional to linear box size. Both the DPM and DLM results converge along approximately straight lines with different slopes to practically the same value.

The variation between the results for the different box aspect ratios is greater for the DPM than for the DLM. However, the DLM results for a particular grid is not always closer to the converged value than the DPM result, in particular for the AR 0.5 series of grids. In the case of the AR 8 series of grids, which may be inappropriate for the DPM considering its single point representation, the convergence behavior of the DPM is not as linear as either the corresponding DLM results or the DPM results for the other series.

70 Degree Delta Wing

Figure 2 shows the convergence history of the pitching moment coefficient of a 70-deg delta wing pitching about the root midchord at $k_r = 2$ and $M = 0.8$. The same paneling schemes that were used in Ref. 7 are used here. The first series of paneling schemes is (span × chord) 10×10, 20×20, 30×30, 40×40, 50×50, 60×60, 70×70, and 80×80. The second series is 5×20, 10×40, 15×60, 20×80, 25×100, 30×120, 35×140, and 40×160, and the third series is 5×50, 10×100, 15×150, 20×200, and 25×250. Equally spaced divisions were used for both the spanwise and the chordwise paneling. The same observations as for the AGARD wing and tail apply.

Circular Wing

Figures 3 and 4 show the unsteady lift and pitching moment coefficients, respectively, for a circular wing pitching about its midchord

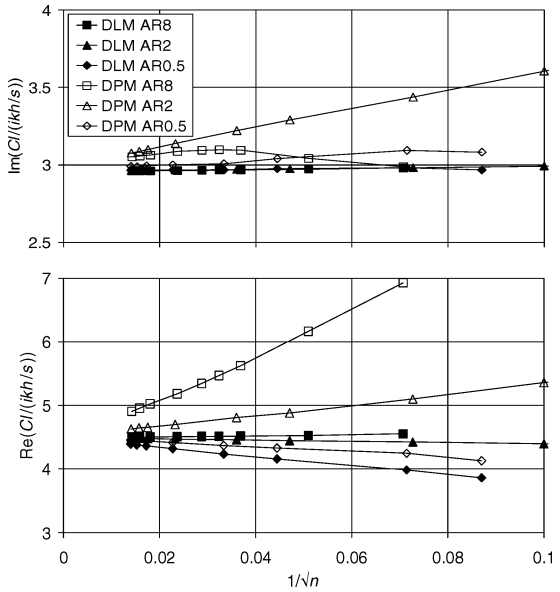

Fig. 1 AGARD wing and tail unsteady lift coefficient at $M = 0.8$ and $k_r = 1.2$.

Received 5 August 2003; revision received 6 October 2003; accepted for publication 16 October 2003. Copyright © 2004 by the American Institute of Aeronautics and Astronautics, Inc. All rights reserved. Copies of this paper may be made for personal or internal use, on condition that the copier pay the $10.00 per-copy fee to the Copyright Clearance Center, Inc., 222 Rosewood Drive, Danvers, MA 01923; include the code 0021-8669/04 $10.00 in correspondence with the CCC.

*Engineer, Defence Aeronautics Programme, P.O. Box 395.
†Director, Air Safety Technology Center. Associate Fellow AIAA.